Arabian Journal of Chemistry (2020) **13**, 5501–5516

King Saud University

Arabian Journal of Chemistry

www.ksu.edu.sa
www.sciencedirect.com

ORIGINAL ARTICLE

Piperine loaded zinc oxide nanocomposite inhibits the PI3K/AKT/mTOR signaling pathway via attenuating the development of gastric carcinoma: *In vitro* and *in vivo* studies

Zhen Yang [a,1,*], Minglong Pu [a,1], Xinhua Dong [a], Feihong Ji [a], Vishnu Priya Veeraraghavan [b], Hongwei Yang [a,*]

[a] *Gastrointestinal Surgery, The First Affiliated Hospital of Zhengzhou University, Zhengzhou, Henan Province, China*
[b] *Department of Biochemistry, Saveetha Dental College, Saveetha Institute of Medical and Technical Sciences, Saveetha University, Chennai 600 077, India*

Received 2 March 2020; accepted 30 March 2020
Available online 9 April 2020

KEYWORDS

Piperine;
Gastric cancer;
Nanocomposite;
AGS cells;
Antioxidant;
Apoptosis

Abstract Gastric cancer (GC) is the fifth most cancer type and the third most cause of cancer-associated deaths worldwide along with the 5-year survival rate is less the 30%. This investigation was aimed to synthesis the piperine-loaded zinc oxide nanocomposite (ZnO-Pip-NC) and investigating its anticancer activity against the GC by *in vitro* and *in vivo* models by the inhibiting the apoptotic and PI3K/Akt/mTOR signaling pathways. The synthesized ZnO-Pip-NC was characterized by different techniques. The cytotoxicity of zinc oxide, piperine and the formulated ZnO-Pip-NC was tested against the AGS cells by MTT assay. The intracellular ROS level, mitochondrial membrane potential, and apoptotic cell necrosis in the AGS cells was examined by fluorescent staining techniques. The expression of apoptotic and PI3K/Akt/mTOR signaling markers were inspected by western blotting and the expression of pro0inflammatory markers analyzed by RT-PCR technique. The antioxidant levels were examined by standard methods and histopathology of gastric mucosa was analyzed. The ZnO-Pip-NC treatment appreciably inhibited the AGS cell viability. ZnO-Pip-NC treated cells also exhibited excessive intracellular ROS, diminished MMP, nuclear damages, and apoptosis induction in AGS cells. The enhanced expression of pro-apoptotic proteins and inhibition of PI3K/Akt/mTOR signaling pathway was noted in ZnO-Pip-NC treated cells. *In vivo* studies proved that the ZnO-Pip-NC noticeably restored the antioxidants in the GC animals and

* Corresponding authors.
E-mail addresses: gegeyang2019@sina.com (Z. Yang), 14988715@qq.com (H. Yang).
[1] Equal contribution.

Peer review under responsibility of King Saud University.

ELSEVIER Production and hosting by Elsevier

https://doi.org/10.1016/j.arabjc.2020.03.028

also prevented the gastric mucosa and inhibited the GC tumor formation. In conclusion, the findings of this investigation confirmed the anticancer potential of ZnO-Pip-NC against the GC via inhibiting the PI3K/Akt/mTOR signaling pathway.

1. Introduction

Gastric cancer (GC) is the fifth most recurrently diagnosed carcinoma and the third foremost cause of cancer-related mortalities worldwide (Torre et al., 2015). In recent decades, the incidences of GC were constantly escalated in East Asian countries. Though the inclusive treatment techniques like chemotherapy, surgery, and endoscopy therapy for the treatment of GC were recently progressed, and the five-year survival rate of GC victims is still unacceptable. The major reason for the treatment failures in GC cases is chemoresistance (Bray et al., 2018). There are numerous molecular mechanisms of gastric cancer was inspected, however, the exact mechanisms of GC like multiplication, migration, progression, and apoptosis are still inadequately understood (Song et al., 2017).

Presently, about 90% of victims were diagnosed with GC was being developed to the developed stage, and the 5-year survival rate in less the 30% (Katai et al., 2018). Preceding findings demonstrated that the incidences and progression of gastric cancer are primarily linked with the mTOR, Nrf2, Wnt, Hedgehog, and Notch signaling hinges (Chen et al., 2018). Presently, the combination of chemotherapy and surgery was executed for the treatment of GC, but the outcome of these techniques is still less enviable. The high toxicity and resistance towards chemotherapy drugs hinder these approaches and hampers the successful recovery of patients from the GC (Lam et al., 2018). Hence, it is essential to explore the potential agents with fewer side effects and improved activity against the GC.

The mTOR is a target of mammalian rapamycin that underwent to an essential function in modulating tumor progressions. The expression of mTOR is frequently uplifted in tumors that consequently suppress autophagy. The significance of mTOR is self evidenced as a crucial element of most signaling pathways and the main inhibitory pathway of autophagy. PI3K/Akt is a typical apoptotic signaling cascade and uplifted signals play an essential regulatory function in the stimulation of mTOR (Kim et al., 2017). The phosphoinositide 3-kinase (PI3K)/Akt (protein kinase B), and the mammalian target of rapamycin (mTOR) signaling pathways are essential for different aspects of physiological and pathological conditions. Because of their close associations, they regularly regarded as a single distinctive pathway that interconnects with various other pathways. The PI3K-AKT-mTOR signaling cascades are among the crucial pathways, which responsible for the drug resistance and directing the mechanisms of carcinoma in cancer victims (King et al., 2015).

PI3K-Akt- mTOR is the critical kinases, which are stimulated via various cellular stimuli and manage the crucial mechanisms of cells, like multiplication, growth, transcription, translation, and survival. The PI3K-Akt-mTOR signaling pathway is very essential for typical human physiological processes; consequently, the alterations in its modulation can lead to numerous carcinomas. To overcome the cellular stresses, the PI3K/Akt signaling pathway is an essential modulator. The interruption during the stimulation of the PI3K/Akt signaling pathway is united with several human malignancies; thus it is an imperative curative target to discover the potential antitumor agents. The function of the PI3K/Akt signaling pathway in the cell multiplication and survival is an extremely critical, and is connected with the autophagy and apoptosis (Yu et al., 2018). Autophagy is a catabolic degradation mechanism that usually engulfs the damaged cell organelles and invading pathogens by lysosomes, digested by its digestive enzymes to maintain the normal cellular processes. Consequently, autophagy has playing the dual functions in the tumor development. It can inhibit the tumor formation via assuaging the accretion of injured organelles and as a molecular mechanism of cell survival; it can eventually escalate the cancer progression. Anomalous autophagy is often concerned in the pathological processes of tumor and even leads to the cancer cell death (Fu et al., 2018). In some cases, autophagy is also involved in drug-induced tumor cell death (Wang et al., 2019; Kinsey et al., 2019). Hence, the recognition of therapeutic agents, which inhibit the PI3K/Akt/mTOR signaling pathway, thereby promoting autophagy and apoptosis may have the potential drug to enhance the effectiveness of GC treatments.

Most of the victims were unavoidably died from the tumor recurrence. Regrettably, there were no efficient curative approaches that exist today to solve this crisis. Currently, the progression of effective curative and preventive methods for the GC is improved but the rate of survival of GC victims was still poor (Siegel et al., 2016). As a result, the need for exploring potential curative approaches is necessary to treat the GC. Piperine is a chief bioactive constituent of black pepper and has been accounted for not only as food ingredient but also as a potential therapeutic agent to treat the diverse ailments like widespread carcinomas, obesity, and inflammation (Bang et al., 2009; Greenshields et al., 2015; Ouyang et al., 2013; Yaffe et al., 2015). Piperine has also reported with the immense pharmacological benefits like anti-epilepsy, anti-depression, and neurodegenerative actions (Chonpathompikunlert et al., 2010; Mao et al., 2014; Ren et al., 2018).

Nanotechnology is a facilitating technology that deals with nano sized materials for the development of novel therapeutic agents (Syafri et al., 2019; Ilyas et al., 2019; Ilyas et al., 2019). Understanding of biological mechanisms on the nano sized agents is a strong driving force behind the emergence of nanotechnology (Ilyas et al., 2018a, 2018b; Abral et al., 2020). Recently, the nanomaterials were gained many interests in biomedical researches that owing to their outstanding biological and biomedical benefits. With the development of nanomaterials, the zinc oxide loaded nanocomposites were received greater importance in the biomedical field, particularly for

anticancer target (Mishra et al., 2017; Zhang et al., 2015, 2014; Wan et al., 2017; Liu et al., 2016; Shi et al., 2017; Huang et al., 2018). The zinc oxide loaded nanocomposites were extensively investigated in numerous fields due to their exclusive chemical and physical properties (Ruszkiewicz et al., 2017). Hence, the current investigation was aimed to synthesis the piperine loaded zinc oxide nanocomposite and exploring its anticancer activity against gastric cancer by *in vitro* and *in vivo* models.

2. Materials and methods

2.1. Chemicals

Piperine (≥97% purity), zinc oxide, Dulbecco's modified eagle medium (DMEM), fetal bovine serum (FBS) (≥98%), dimethyl sulfoxide (DMSO) (≥99.9%), 3-(4,5-dimethylthia zol-2-yl)-2,5-diphenyl tetrazolium bromide (MTT), Dichloro-dihydro-fluorescein diacetate (DCFH-DA) (≥97%), Rhodamine-123 (≥85%), acridine orange, ethidium bromide (≥95%), 4′,6-diamidino-2-phenylindole (DAPI) (≥98%), and propidium iodide (≥94%) was attained from Sigma Aldrich, USA. All the antibodies from western blotting and PCR kit were procured from Thermo-fisher scientific, Waltham, USA. The extraction kits were purchased from Qiagen, Hilden, Germany. All additional chemicals were attained from Himedia, USA, as a diagnostic grade.

2.2. Synthesis of piperine-loaded zinc oxide nanocomposite (ZnO-Pip-NC)

To synthesize the ZnO-Pip-NC, 1gm of ZnO powder was suspended in 100 ml of acetic acid (1%) to develop the zinc cations. Then 1gm of piperine was added to this suspension and then constantly sonicated in a water bath for 2 h. The 1 M of NaOH solution was added by dropwise manner to gain the pH 9. Afterward, the changing of its color from pale yellow to deep brown was noted. Finally, the nanocomposite solution was centrifuged at 6000 rpm for 5mins and then the pellet was gathered. The resulted ZnO-Pip NC was dried at 40 °C and further characterized by different techniques.

2.3. Characterization of synthesized ZnO-Pip-NC

The formation of ZnO-Pip-NC in the sample was confirmed by the UV–vis spectroscopic (Shimadzu UV 2600 plus) analysis was executed at the wavelength range from 200 to 1100 nm to confirm the formation of ZnO-Pip-NC in the solution (Reda et al., 2020). The Fourier Transform Infrared Spectroscopy (spectrum GX-1, Perkin Elmer, USA) technique was executed to inspect the stretching and bending vibrations of the ZnO-Pip-NC within the wavelength range from 400 to 4000 cm^{-1}. The phase level was investigated via the X-ray diffraction (Bruker D8 X-ray diffraction) with Cu-K alpha x-ray radiation, a tube voltage of 40 kV, a current of 40 mA were used, a 0–80° scanning angle, and a scanning rate (2Θ) of 0.02°. The average size of the fabricated ZnO-Pip-NC was studied through the transmission electron microscopy (FEI-G220), operating at 200 kV, with a resolution point of 2.04 nm. The photoluminescence property of the formulated ZnO-Pip-NC was investigated through the spectrofluorimeter at the wavelength ranging from 340 to 800 nm (PerkinElmer, Waltham, USA).

2.4. Cell culture

Gastric cancer (AGS) cell lines were procured from ATCC, USA. Cells were maintained in DMEM medium along with 10% FBS and 1% Penicillin/Streptomycin combination at 37 °C in a moistened atmosphere having 5% CO_2 and 95% air incubation.

2.5. MTT cytotoxicity assay

The cytotoxicity potential of formulated ZnO-Pip-NC was inspected through MTT based colorimetric assay. AGS cell lines were loaded in 96-well plates 6×10^3 cells/well and maintained at 37 °C for 24 h at 37 °C. To examine the cytotoxicity of ZnO-Pip-NC, it was supplemented in diverse doses (5–35 μM) to the AGS cells and incubated for 24 h at 37 °C. Later than 24 h incubation, the 100 μl of MTT solution was added to every well and then plates were again kept for incubation for 4 h. Then the growth medium was discarded from every well and 100 μl of the serum-free medium was replenished and developed formazan crystals were liquefied via adding DMSO. Finally, the absorbance was taken by the microplate reader at 570 nm.

2.6. Cell proliferation assay

The effect of formulated ZnO-Pip-NC against the AGS cells was examined. Briefly, the AGS cells were loaded in the 6-wellplate at 1×10^6 cells/well population and sustained for 24 h at 37 °C. Then the growth medium was re-supplemented with fresh medium along with the diverse doses of ZnO-Pip-NC (15 & 20 μM/ml). The medium (excluding the ZnO-Pip) was utilized as control and incubated at 24 h at 37 °C. Later than, cells were gathered and cleaned with distilled water and finally the cell proliferation level was examined beneath the inverted optical microscope.

2.7. Measurement of intracellular ROS production

Intracellular ROS accretion status was inspected via DCFH-DA fluorescent staining technique. Briefly, GC (AGS) cells were loaded in a 6-wellplate and supplemented with various doses (15 and 20 μM) of formulated ZnO-Pip-NC, and then kept incubation for 24 h in a CO_2 chamber at 37 °C. Subsequently, cells were stained with DCFH-DA and kept incubation for another 10 min. Later than, the fluorescent intensity was inspected via a fluorescent microscope at 530 nm emission filters.

2.8. Detection of mitochondrial membrane potential (MMP)

MMP level was examined through the Rhodamine-123 (Rh-123) fluorescent staining technique. The AGS cells were cultured in 6-wellplate along with the supplementation of diverse dosages of fabricated ZnO-Pip-NC (15 and 20 μM). After that, treated cells were incubated for 30 min with Rh-123 fluorescent stain. Finally, the changes in the MMP were inspected through the fluorescent microscopy.

2.9. Detection of cell death by the dual staining method

The dual staining technique i.e. acridine orange (AO)/ethidium bromide (EB) was executed to recognize the cellular apoptosis in AGS cells. The formulated ZnO-Pip-NC supplemented (15 and 20 μM) AGS cells were incubated for 24hrs and then cells were stained with AO/EB for 30mins. Finally, the cells were instantly investigated via the fluorescent microscope to detect cell death.

2.10. Detection of DNA fragmentation

The AGS cells were loaded at the 6-wellplates and incubated for 24hr at 37 °C along with the diverse doses (15 and 20 μM) of formulated ZnO-Pip-NC. Then the cells were harvested and cleaned with chilled PBS to attain the 500 μl of cell suspension. After that, 1 μg/ml of DAPI dye was added incubated for 10mins at 37 °C. Finally, the DNA fragmentation was inspected beneath the fluorescence microscope at excitation 358 nm and emission 460 nm).

2.11. Detection of cell apoptosis

The propidium iodide (PI) staining approach was extensively executed to stain the cells to detect the cellular morphology. PI stain incapable to penetrate into the live cell membrane, thereby clearly distinguish the apoptotic and normal viable cells. After 12hr of incubation with fabricated ZnO-Pip-NC (15 and 20 μM), the AGS cells were gathered and centrifuged at 3000 rpm for 6mins and then cleaned with PBS twice. Later than, cells were treated with 3 ml of 75% chilled ethanol at 4 °C for 12hr. Then, cells were treated with10μl of RNase at 37 °C for 10mins. Subsequently, AGS cells were stained with 1% of PI and investigated via the fluorescent microscope.

2.12. Western blotting analysis

The total protein was extracted and quantified from the 15 and 20 μM of ZnO-Pip NC supplemented AGS cells with the help of a protein extraction kit (Qiagen, Hilden, Germany). The extracted protein from the cells was separated via SDS-PAGE technique and repositioned to the PVDF membrane. Then the membranes were blocked with fat less milk concentrate (5%) at 37 °C for 1 h. After that, the membranes were processed with saline solution and Tween 20 (0.1%), and then membranes were incubated at 4 °C with the BSA (5%) and corresponding primary antibodies (Thermo-fisher scientific, Waltham, USA). Subsequently, membranes were incubated again with fat less milk (5%) and horseradish peroxidase loaded secondary antibodies. Finally, the developed bands were inspected through the enhanced chemiluminescence kit (Thermo-fisher scientific, USA). The β-actin was utilized as a control.

2.13. Real-time polymerase chain reaction (RT-PCR) analysis

The total RNA was extracted from the control and ZnO-Pip-NC supplemented AGS cells via the TRIzol RNA extracting kit by using the manufacturer's protocol (Qiagen, Hilden, Germany). The cDNA was constructed from the extracted RNA through the commercially procured PCR kit as per the manufacturer's guidelines (Thermo-fisher scientific, Waltham, USA). The primers used for the TNF-α was as forward 5-CTGAACTTCGGGGTGATCG-3 and reverse 5-GCTTG GTGGTTTGCTACGAC-3, NF-ƙB forward 5′-ATCC CATCTTTGACAATCGTGC-3′, reverse 5′-CTGGTCCCGT GAAATACACCTC-3′, forward 5-ATCATTCACCAGGC AAATTGC-3, reverse: 5- GGCTTCAGCATAAAGCG TTTG-3, and β-actin forward 5-GCTCCTCCTGAGCGCAA GT-3, reverse 5-TCGTCATACTCCTGCTTGCTGAT-3 was used. The entire investigation was executed in triplicate for an exact result.

2.14. In vivo studies

2.14.1. Experimental design

The investigation was executed in Wistar albino rats (male breed) with weight ranges from 6 to 8 weeks. Rats were alienated into 4 groups with 6 animals in every group. Group-I regarded as control with excluding the experimental procedures. Group-II were challenged with 200 mg/kg bw of N-Methyl-N′-nitro-N-nitrosoguanidine (MNNG) by oral gavage route at days 0 and 14th day and saturated NaCl (1 ml per rat) was administered for 3 days for 4 weeks and sustained till the end of the investigational period. Group-III and IV were challenged with MNNG + NaCl (as mentioned in group-II) and supplemented with 10 and 20 mg/kg bw of ZnO-Pip-NC respectively for 20 weeks from the first dose of MNNG + NaCl. After completion of the investigational schedule, all rats were anesthetized and killed via cervical decapitation then samples were gathered and utilized for biochemical and histological examinations. The body weight, tumor volume, and incidences of GC were investigated via the previously described method (Wang and Williams, 1995) (Wang and Williams, 1987).

2.14.2. Biochemical assays

The 0.6 g of detached stomach tissues were homogenized with the 9 ml of saline solution and centrifuged at 10,000 rpm for 6 min to attain the 10% of stomach tissue homogenate. The resulted stomach tissue homogenate was utilized for the different biochemical assays. The lipid peroxidation level in the stomach tissues was inspected through the spectrophotometrical technique by assaying the status of thiobarbituric acid reactive substances (TBARS) by the method of Niehius and Samuelson, (Niehius and Samuelson, 1968). The status of enzymatic antioxidants i.e. superoxide dismutase (SOD), catalase (CAT), and glutathione peroxidase (GPx) was inspected through the preceding techniques described by Kakkar et al. (1984); Sinha (1972), and Rotruck et al. (1973) respectively. The glutathione (GSH) status was examined via the Ellman (1959) procedure. The vitamin-C and vitamin-E statuses were examined via the procedures of Omaye et al. (1979) and Desai (1984) respectively.

2.15. Histological analysis

The histological alterations in the stomach tissues of control and investigational animals were studied via hematoxylin and eosin (H&E) staining. The gathered stomach tissues were fixed in 10% of formalin solution for overnight and dehydrated with the help of alcohol and xylene. The dehydrated tissues were entrenched in paraffin and then sliced at 5 μm size.

The sliced sections were stained with H&E and finally, the sections were inspected beneath the optical microscope.

2.16. Statistical analysis

Data were investigated statistically through the SPSS version 18 statistical software. Data were illustrated as mean ± SD of triplicate tests. The one way ANOVA test subsequently DMRT study was executed to examine the variations among the groups. A p-value less than 0.05 regarded as significant.

3. Results

3.1. Characterization of synthesized ZnO-Pip-NC scaffold

As depicted in Fig. 1A, three distinct peaks were noted at 305, 340, and 1008 nm. These peaks were proved the formation of ZnO-Pip-NC. Fig. 1B reveals the photo-luminescent spectrum of the fabricated ZnO-Pip-NC scaffold. The photoluminescence spectrum was clearly displayed the distinct and maximum peak in a wavelength interval at 644.96 nm. It was confirmed the photo-luminescent property of the formulated ZnO-Pip-NC scaffold.

Fig. 2A shows the FT-IR spectrum of ZnO-Pip-NC and revealed the diverse incorporation of peaks ranging from 3438 to 604.32 cm^{-1}. The peak at 3438 cm^{-1} denotes the existence of OH stretching and also the existence of amino acids. The frequencies of 2922, 2863, and 2094 cm^{-1} denoted the CH stretching in the nanocomposite. The peaks at the 1633 cm^{-1} are indicating the amide group and CO extensions. The 1448 and 1383 cm^{-1} peaks were denoting the sulfur residues. The peak at 604.32 cm^{-1} is a characteristic absorption of Zn–O bond. The frequencies range from 1250, 1095, 1032 cm^{-1} peaks were denoting the amino acids.

The DLS study was executed to inspect the size and distribution of the formulated ZnO-Pip-NC scaffold (Fig. 2B). The findings of DLS revealed the single highest peak with an average size of 626.5 nm along with a narrow distribution.

The crystalline phase of formulated ZnO-Pip-NC inspected via X-ray diffraction analysis. The attained XRD pattern was illustrated in Fig. 3A, and it revealed the typical metallic ZnO-Pip-NC. The distinct narrow peak of the XRD pattern of ZnO-Pip denotes the crystallized nature.

The average size of the fabricated ZnO-Pip-NC scaffold was inspected through the TEM analysis and the images were illustrated in Fig. 3B. The TEM images of formulated ZnO-Pip-NC has demonstrated the distinct dark spots with a spherical shape that proved the occurrence of ZnO-Pip-NC with size ranges from 40 to 90 nm (Fig. 3B).

3.2. Effect of ZnO and piperine against the viability of gastric cancer cell (AGS) lines

The MTT cytotoxicity assay was executed to notice the cytotoxic effect of ZnO and the piperine against the viability of gastric cancer (AGS) cells and the results were illustrated in the Fig. 4(A&B). The viability of AGS cell was noticeably decreased after the treatment with the piperine in a dose dependant manner (Fig. 4B). The piperine treatment was exhibited the notable cytotoxicity against the AGS cells than the ZnO treatment.

3.3. Effect of ZnO-Pip-NC scaffold against the AGS cell viability and proliferation

The potential cytotoxicity of the formulated ZnO-Pip-NC scaffold against the AGS cells was investigated by the MTT

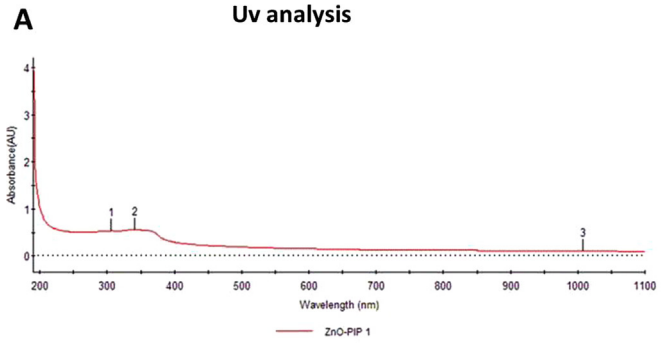

Name	No.	Peak(nm)	Peak(AU)
ZnO-PIP	1	305.90	0.5359
	2	340.55	0.5609
	3	1,008.20	0.1113

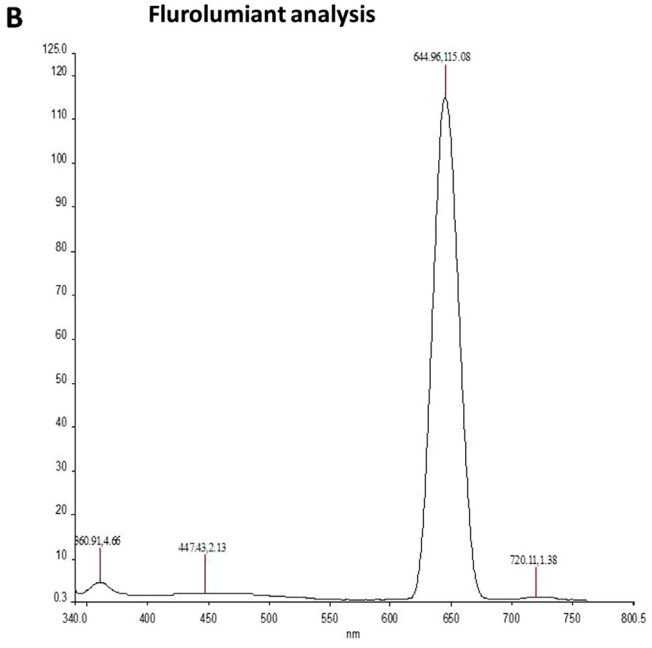

Fig. 1 Characterization of synthesized ZnO-Pip-NC scaffold. UV–vis spectral analysis of synthesized ZnO-Pip-NC demonstrates three distinct peaks at 305, 340, and 1008 nm, which confirmed the formation of ZnO-Pip-NC (Fig. 1A). The photoluminescence spectrum displayed a distinct peak at a wavelength of 644.96 nm (Fig. 1B).

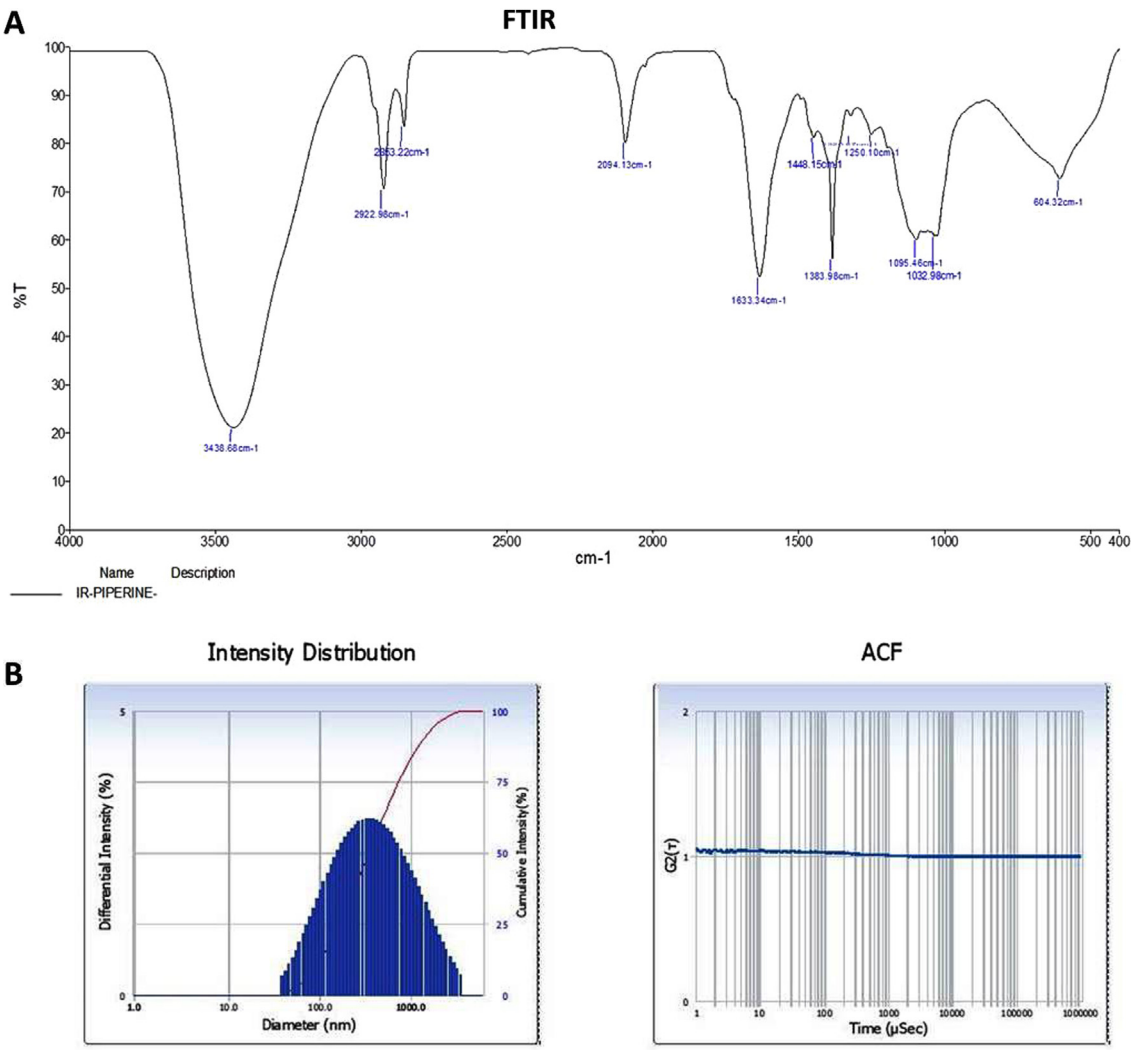

Fig. 2 Characterization of synthesized ZnO-Pip-NC scaffold. The FT-IR peaks confirmed the presence of different functional groups in the synthesized ZnO-Pip-NC (Fig. 2A). The result of DLS study revealed the highest peak with an average size 626.5 nm along with dispersed nature of the ZnO-Pip-NC (Fig. 2B).

assay. Fig. 5A revealed that the ZnO-Pip-NC scaffold was substantially inhibited the AGS cell viability at the dose-dependent mode; merely the augmented dose of ZnO-Pip-CN exhibited enhanced cytotoxicity against the AGS cells. The ZnO-Pip NC was supplemented in various concentrations (5–35 µM) and the 20 µM of ZnO-Pip-NC was inhibited 50% of cell growth. In that way, the 20 µM of ZnO-Pip-NC was opted as IC_{50} and utilized for the additional investigations. Subsequently, the ZnO-Pip-NC was also investigated for its synergistic effect on the cell proliferation of AGS cells. The morphological investigation displayed the drastic alterations in the cell proliferation level of the AGS cells. The proliferation level of the control cells was distinctly differed from the 15 and 20 µM of the ZnO-Pip-NC supplemented cells (Fig. 5B). The ZnO-Pip-NC treatment displayed tremendous morphological alterations like unequal shape, roundings, cell shrinkages, and detachments when compared to the control.

3.4. Effect of ZnO-Pip NC scaffold on the intracellular ROS level in AGS cells

Fig. 6 proved that the ZnO-Pip-NC treatment noticeably elevated the intracellular ROS production in the AGS cells. A bright green fluorescent in the 15 and 20 µM ZnO-Pip-NC treated cells were revealing the enhanced accumulation of intracellular ROS, thereby, promoting the apoptotic mechanisms in the AGS cells. The untreated control cells exhibited none green fluorescence that indicating the stimulation of too much intracellular ROS production in AGS cells by the ZnO-Pip-NC treatment.

3.5. Effect of ZnO-Pip-NC scaffold on mitochondrial membrane potential (MMP) and nuclear fragmentation in the AGS cells

The alterations in the MMP of ZnO-Pip-NC supplemented AGS cells were examined through the Rhodamine-123 fluores-

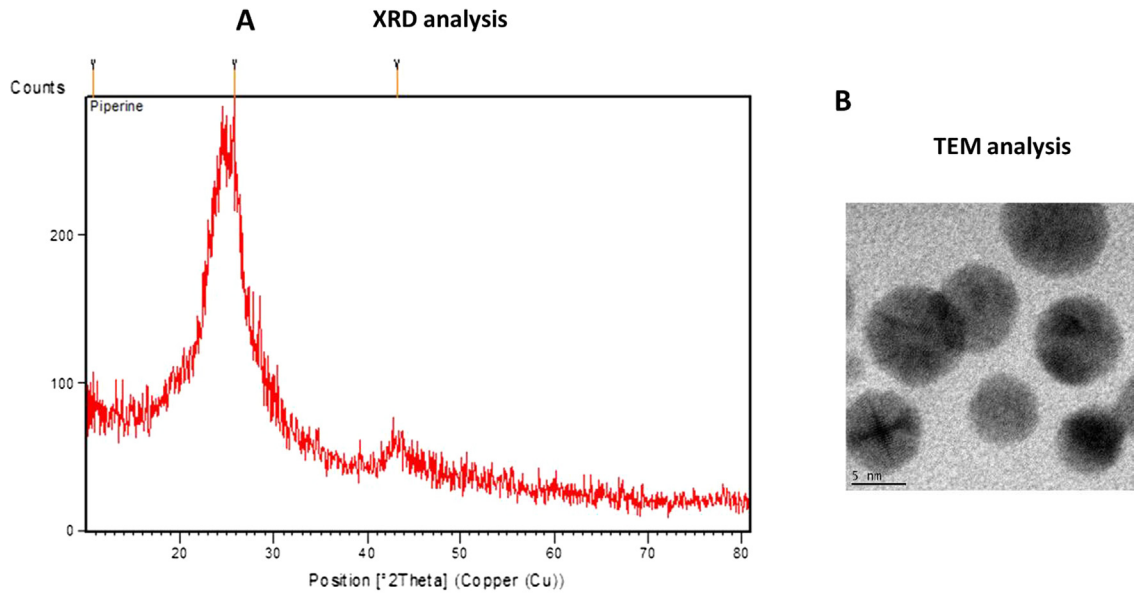

Pos. [°2Th.]	Height [cts]	FWHM Left [°2Th.]	d-spacing [Å]	Rel. Int. [%]
10.7985	6.55	0.7872	8.19313	5.02
25.8190	130.54	0.9840	3.45075	100.00
43.1847	17.05	1.9680	2.09494	13.06

Fig. 3 Characterization of synthesized ZnO-Pip-NC scaffold. Fig. 3A illustrates the XRD patterns that prove the crystallinity of formulated ZnO-Pip-NC. The TEM images of formulated ZnO-Pip-NC showed the spherical shape with the average size ranges from 40 to 90 nm (Fig. 3B).

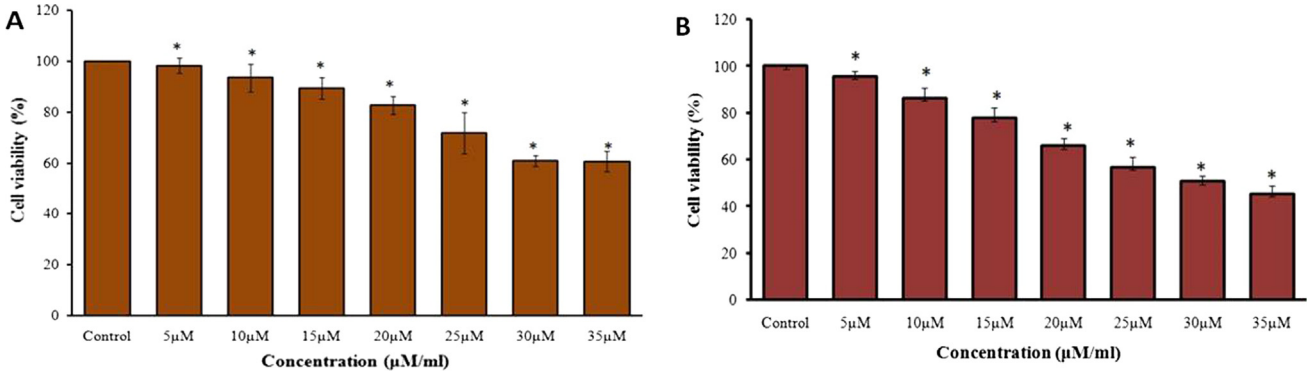

Fig. 4 Effect of ZnO and piperine against the AGS cell line viability. As mentioned in the Fig. 5, the treatment with the ZnO and piperine showed the decreased viability of gastric cancer (AGS) cells. The piperine treatment showed the prominent cytotoxicity to the AGS cancer cells than the ZnO.

cent staining method. The augmented MMP levels in the cells develop a strong green fluorescence while the decreased MMP displays dull or slight fluorescence, which indicates the disaggregated cells. As depicted in Fig. 7, the control cells displayed the intense green fluorescence, while the ZnO-Pip-NC supplemented AGS cells demonstrated the very minimal green fluorescence, which evidencing the declined MMP on ZnO-Pip-NC treated AGS cells. The ZnO-Pip-NC supplemented AGS cells were examined by the DAPI fluorescent staining. The microscopic images were revealed the noticeable alterations in the nuclear morphology than the control cells. The intense blue fluorescence was noted on the ZnO-Pip-NC supplemented AGS cells than the untreated control cells, which confirms the nuclear damage in the AGS cells thereby inducing cell death (Fig. 7).

3.6. Effect of ZnO-Pip-NC scaffold on DNA damage and cell necrosis in the AGS cells

The DNA damage and the level of cell necrosis in the ZnO-Pip-NC treated AGS cells were inspected via dual (AO/EtBr) staining and PI staining techniques respectively.

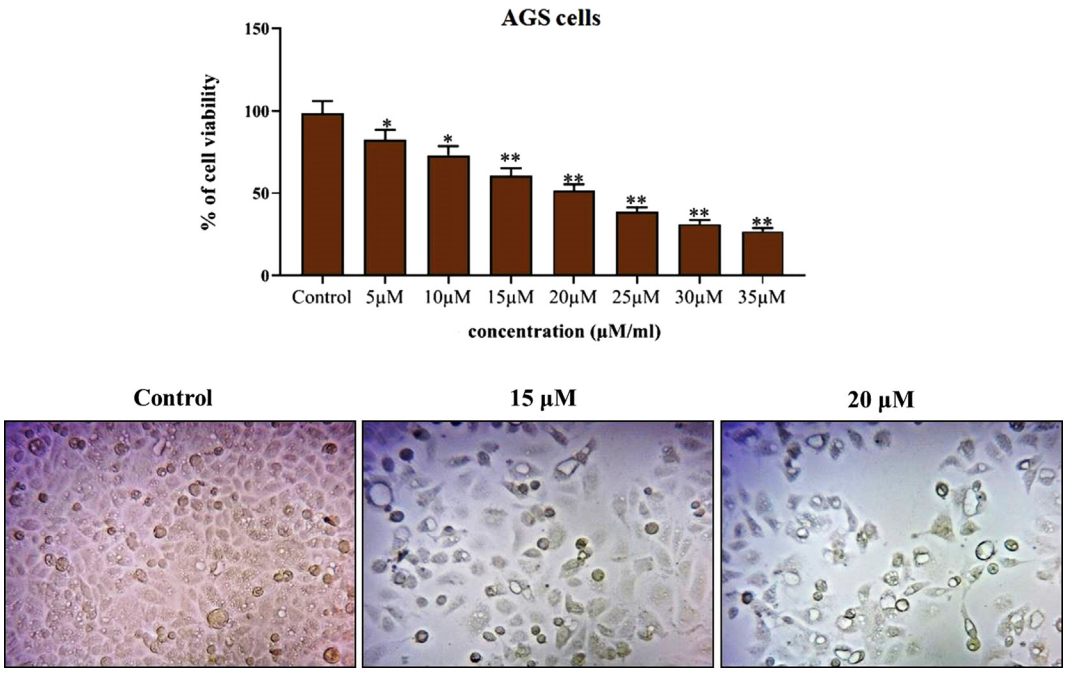

Fig. 5 Effect of synthesized ZnO-Pip-NC scaffold against the viability and proliferation of AGS cell line. Fig. 6 proved the significant cytotoxicity of ZnO-Pip NC against the AGS cells. Among the different concentrations (5–35 μM), the 20 μM of ZnO-Pip-NC was inhibited 50% of cell growth (IC_{50}).

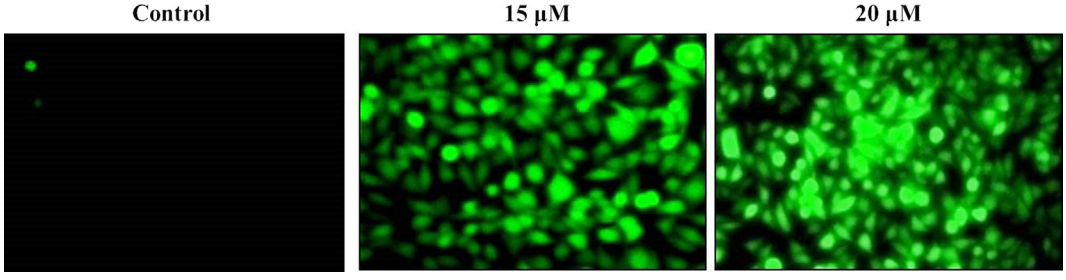

Fig. 6 Effect of synthesized ZnO-Pip NC scaffold on intracellular ROS level in the AGS cells. The bright green fluorescent exhibited by the 15 and 20 μM ZnO-Pip-NC treated cells than the control was proves the enhanced accumulation of intracellular ROS in the AGS cells.

The microscopic images of dual staining were depicted in Fig. 8, which revealed that the untreated control cells were displayed the AO stained green fluorescence; surprisingly the ZnO-Pip-NC supplemented AGS cells were demonstrating the intense EtBr stained orange fluorescence. This outcome indicated severe DNA damage. The PI stained AGS cells exhibited the bright red color fluorescence when compared to the control cells, which evidenced the increased necrotic cells. Both concentrations (15 and 20 μM) of ZnO-Pip-NC has enthused the apoptosis in gastric cancer (AGS) cells. These results proved that the ZnO-Pip-NC supplementation enhanced the DNA damage thereby cell necrosis in gastric cancer (AGS) cells.

3.7. Effect of synthesized ZnO-Pip-NC on the apoptotic protein expressions

As depicted in Fig. 9, the drastic diminution in the expressions of pro-apoptotic proteins like p53, Bad, PARP, caspase-3 and -9 and a noticeable increase in the anti-apoptotic protein expressions i.e. Bcl-2 was noted in the control gastric cancer (AGS) cells (Fig. 9). Interestingly, the ZnO-Pip-NC supplemented AGS cells were displayed the noticeable improvement in the pro-apoptotic protein expressions like p53, Bad, PARP, caspase-3 and -9, also diminished the over-expression of anti-apoptotic protein expression i.e. Bcl-2, while comparing it to the control cells. By this means, it was clear that the formulated ZnO-Pip-NC can trigger apoptosis in the human gastric cancer (AGS) cells (Fig. 9).

3.8. Effect of ZnO-Pip-NC in the activation of PI3K/Akt/mTOR signaling pathway

The expression of the mammalian target of rapamycin (mTOR) is normally uplifted in the tumor cells to inhibit autophagy. PI3K/Akt, a component upstream of mTOR, takes a crucial regulatory function in the stimulation of mTOR. Hence, we investigated the relationships between the formulated ZnO-

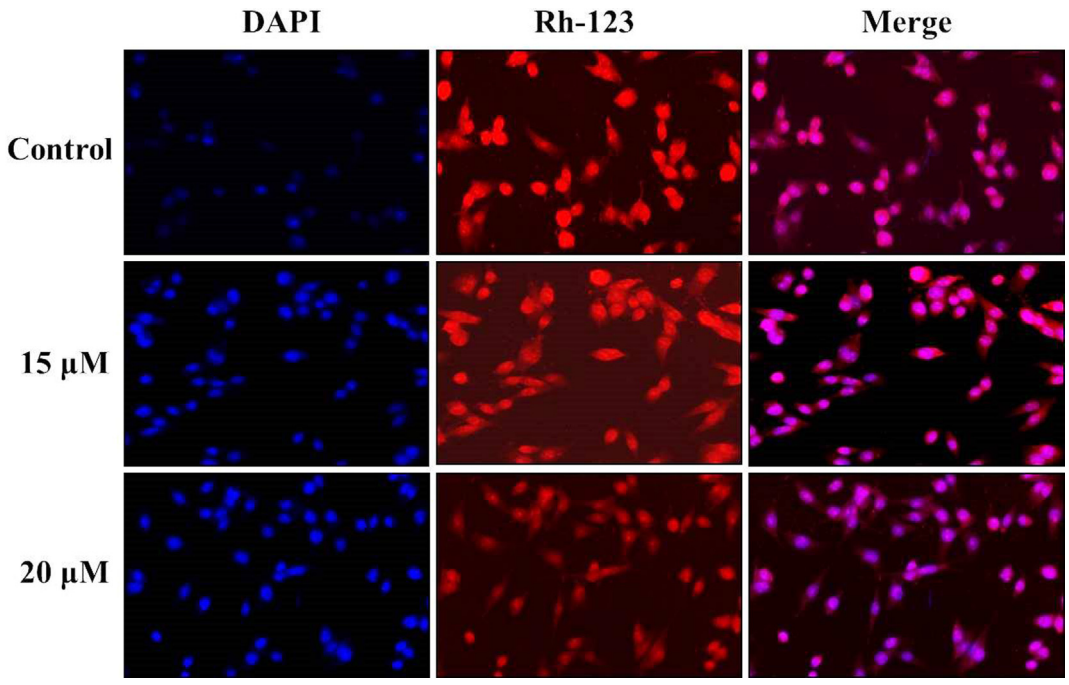

Fig. 7 Effect of synthesized ZnO-Pip-NC on the mitochondrial membrane potential (MMP) and nuclear fragmentation in the AGS cells. As depicted in Fig. 8, the ZnO-Pip-NC supplemented AGS cells demonstrated the very minimal green fluorescence than the control cells that evidencing the declined MMP on ZnO-Pip-NC treated AGS cells. The intense blue fluorescence was noted on the ZnO-Pip-NC supplemented AGS cells than the untreated control, which confirms the nuclear damages.

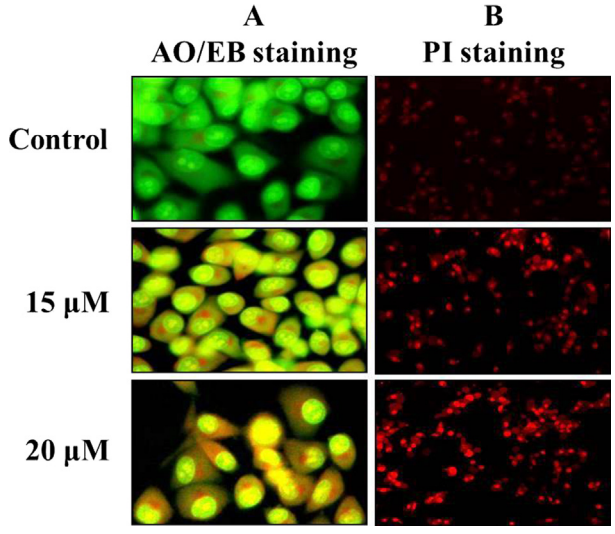

Fig. 8 Effect of synthesized ZnO-Pip-NC scaffold on DNA damage and cell necrosis in the AGS cells. Fig. 9 revealed that the control cells were displayed the AO stained green fluorescence; surprisingly the ZnO-Pip-NC supplemented AGS cells were demonstrating the intense EtBr stained orange fluorescence that conforms the severe DNA damage. The PI stained AGS cells revealed that the ZnO-Pip-NC has stimulated the apoptosis in gastric cancer (AGS) cells.

Pip-NC triggered autophagy and the PI3K/Akt/mTOR signaling pathway. The result of western blotting exhibited a notably reduced phosphorylation of mTOR than the untreated control cells (Fig. 10). The ZnO-Pip-NC treatment also suppressed the expression of Akt in the AGS cancer cells. This outcome proved that the ZnO-Pip-NC treatment to the AGS cells inhibited the PI3K/Akt/mTOR signaling pathway, thereby promoted autophagy in gastric cancer (AGS) cells.

3.9. Effect of ZnO-Pip-NC on body weight, tumor weight, and tumor incidence in the experimental animals

Table 1 revealed that the MNNG provoked GC in animals were resulted in the severely diminished bodyweight and augmented tumor weight and incidences while comparing it to control. Conversely, the supplementation of formulated ZnO-Pip-NC to the MNNG-stimulated animals displayed the notable body weight gain, when compared to the GC induced animals. The ZnO-Pip-NC supplemented animals also diminished the tumor volume and tumor incidences, which is contrary to the MNNG-triggered animals. The supplementation of 20 mg/kg of formulated ZnO-Pip-NC to the animals did not exhibit any weight loss and tumor incidences. The results of ZnO-Pip-NC supplemented animals were completely similar to the control group.

3.10. Effect of ZnO-Pip-NC on TBARS and antioxidant enzymes level in the experimental animals

The MNNG-stimulated GC in the investigational animals displayed the drastic escalation in the TBARS level and also severely diminished the status of enzymatic antioxidants like SOD, CAT, and GPx in stomach tissues of MNNG-challenged animals when compared with the control.

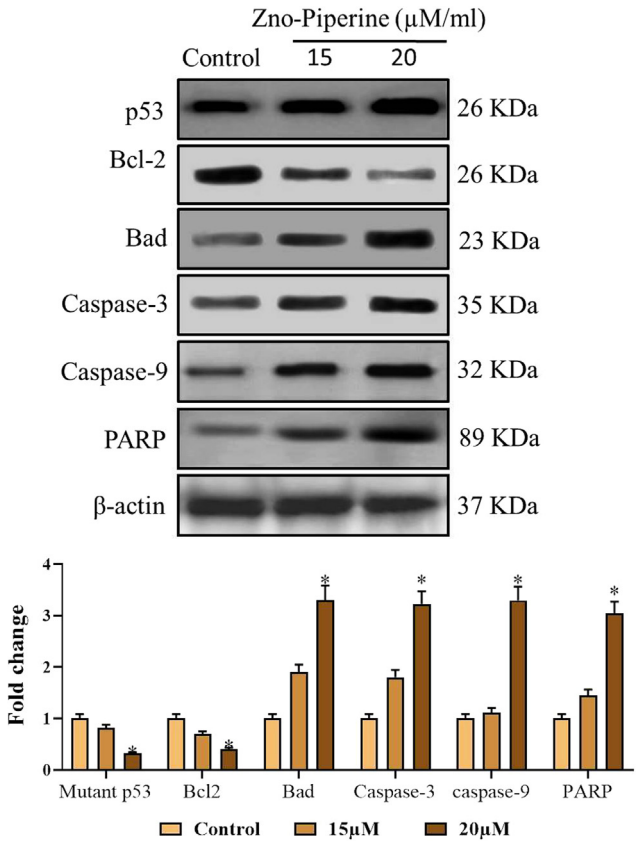

Fig. 9 Effect of synthesized ZnO-Pip-NC on the apoptotic protein expressions. The ZnO-Pip-NC supplemented AGS cells were displayed the appreciable enhancement in the pro-apoptotic protein expressions i.e. p53, Bad, PARP, caspase-3 and -9, also diminished the excess expression of anti-apoptotic protein expression i.e. Bcl-2 in the AGS cells.

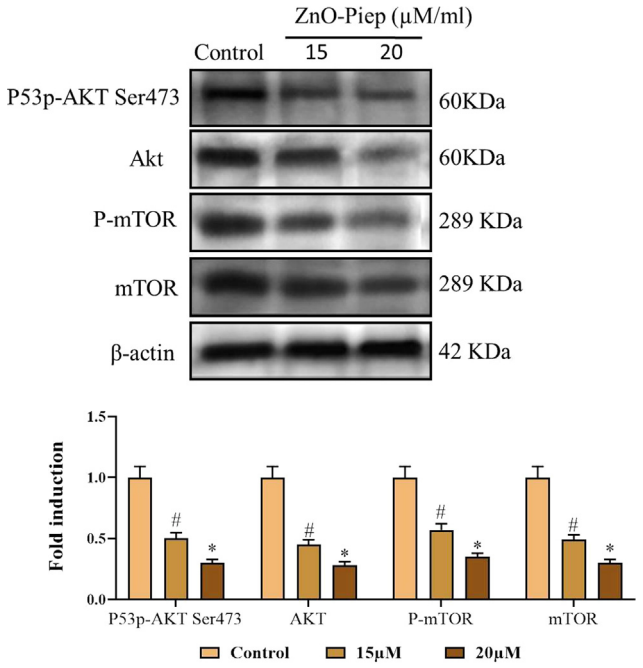

Fig. 10 Effect of synthesized ZnO-Pip-NC in the activation of PI3K/Akt/mTOR signaling pathway. The reduced phosphorylation of mTORwas noted in the ZnO-Pip-NC treated AGS cells than the untreated control cells. ZnO-Pip-NC treatment also suppressed the expression of Akt in the AGS cancer cells.

Interestingly, the 10 and 20 mg/kg of the ZnO-Pip-NC supplementation to the GC induced animals have appreciably regained the antioxidant enzyme status in the stomach tissues (Fig. 11). The pre-treatment with the ZnO-Pip-NC subsequently MNNG challenge was appreciably escalated the antioxidant enzyme status i.e. SOD, CAT, and GPx in the stomach tissues of the investigational animals. This outcome confirmed the antioxidant potential of the formulated ZnO-Pip-NC. The result of the ZnO-Pip-NC treatment and control group were similar to each other.

3.11. Effect of ZnO-Pip-NC on the non-enzymatic antioxidants level in the experimental animals

The MNNG challenged GC in the animals displayed the drastic diminution in the non-enzymatic antioxidants i.e. GSH, vitamin-C, and vitamin-E in the stomach tissues when compared with the control animals. Conversely, the 10 and 20 mg/kg of ZnO-Pip-NC treated animals amazingly recovered the non-enzymatic antioxidants like vit-E, vit-C, and GSH in the stomach tissues, which in contrast to the MNNG-challenged animals. The control and ZnO-Pip-NC supplemented animals displayed similar kinds of outcomes (Fig. 12).

3.12. Effect of ZnO-Pip-NC on histological analysis of gastric mucosa in the experimental animals

The Histopathological investigation of the gastric mucosa of MNNG stimulated GC animals have displayed a severe histological alteration when compared to the control. Gastric mucosa of MNNG-stimulated animals exhibited an invasion of carcinogenic cuboidal epithelial cells to the submucosal layer gastric mucosa. The inflamed lamina propria, unsystematic glands and dysplastic glands in the gastric mucosa of the MNNG challenged animals. Interestingly, the treatment with the 10 and 20 mg/kg of the formulated ZnO-Pip-NC to the MNNG-challenged animals has noticeably ameliorated the histological changes and alleviated the burden of gastric cancer (Fig. 13).

4. Discussion

GC is a major one among the aggressive cancers, and it remained with the reduced survival rate due to the late diagnosis and pertained resistance towards the existing chemotherapeutic drugs (Nienhuser and Schmidt, 2018). Consequently, the exploration of potential treatment approaches was needed to avert the progression of GC. The high incidences of mutations were linked with the PI3K-Akt-mTOR signaling pathways and the genetic alterations in the PI3K-Akt-mTOR signaling pathway were directly influence in the progression of many cancers (Aziz et al., 2018). The PI3K/Akt signaling pathway is a crucial signaling cascade, which modulates cellular apoptosis. The PI3K is an intracellular phosphatidylinositol kinase and Akt, also recognized as a protein kinase-B, is

Table 1 Effect of ZnO-Pip-NC on body weight, tumor weight, and tumor incidence in the experimental animals.

Groups	Body weight (gm)	Tumor weight (gm)	Number of rats with gastric cancer (%)
Group I	**315.90 ± 28.42**	**0**	**0**
Group II	**165.15 ± 14.86**	**0.75 ± 0.07**	**6(100%)**
Group III	**250.49 ± 22.54**	**0.28 ± 0.03**	**2**
Group IV	**275.99 ± 24.83**	**0**	**0**

The ZnO-Pip-NC supplementation to the GC stimulated animals appreciably regained the body weight. The ZnO-Pip-NC treatment also suppressed the tumor volume and tumor incidences in the GC induced experimental animals.

a serine/threonine kinase, which is a prime downstream target of the PI3K signal transduction pathway. The PI3K/Akt pathway influences the downstream effector molecule statuses as a critical intracellular signaling cascade, which performs an essential function in modulating apoptosis. This pathway is directly linked to the progression of numerous human cancers (Zheng et al., 2015). Due to gaining a much interests, the green chemistry aims to produce cost effective, high efficient and safer nano agents for the numerous therapeutic applications (Zhang et al., 2014; Liu et al., 2015, 2009; Shi et al., 2017; Ramirez et al., 2020). The formulation of non-toxic nano materials by green route has become a popular approach among the researchers. The reduction of particle size is a general method to enhance the drug solubility by enlarging the surface area (Reda et al., 2020; Huang et al., 2018). In this current investigation, the formation of ZnO-Pip-NCs were identified through the V-vis spectroscopic study (Fig. 1A), the noticed peaks at 305, 340, and 1008 nm were confirmed the same. The FT-IR spectrum of ZnO-Pip-NC (Fig. 2A) was revealed the diverse frequencies that directly indicate the presence of amide group, CO extensions, sulfur residues, and amino acids in the formulated ZnO-Pip-NC. The findings of DLS study (Fig. 2B) revealed the single highest peak with an average size of 626.5 nm along with a narrow distribution. Fig. 3 proved that the formulated ZnO-Pip-NC has the typical metallic nature. The distinct narrow peak of the XRD pattern of ZnO-Pip denotes the crystallized nature. We evidenced that the treatment with formulated ZnO-Pip-NC substantially inhibited the stimulation of Akt protein expressions, as confirmed via the diminished expressions of these proteins. Hence it was clear that the fabricated ZnO-Pip-NC was appreciably enhanced the apoptosis through inhibiting the PI3K/Akt signaling pathway.

Autophagy is a non-apoptotic form of programmed cell death known as autophagy-mediated cell necrosis. In recent times, autophagy has appeared as a crucial target in cancer researches (Huang et al., 2018). The biological mechanisms of autophagy in the cancer cells are highly complex and its stimulation or inhibition is concerned in the major event in the cancer cells (Yao et al., 2017). The stimulation of autophagy in the cancer cells can result in the autophagy-regulated tumor cell necrosis (Clavel et al., 2017). The autophagy is a type-2 programmed cell necrotic mechanism that closely connected but dissimilar from apoptosis, has turned into an emerging topic in cancer research (Jeong et al., 2019). Furthermore, the connection between autophagy and apoptosis is controversial. Autophagy could inhibit apoptotic cell death; though, autophagy and apoptosis can also cooperate as allies to promote the cell death (Galluzzi et al., 2017). In this investigation, the findings were proved the apoptosis and autophagy stimulating capacity of the formulated ZnO-Pip-NC against the human gastric cancer (AGS) cells. The ZnO-Pip-NC supplemented AGS cells were displayed enhanced apoptosis as well as autophagy-mediated cell necrosis in the AGS cells as confirmed by the different fluorescent staining techniques. These findings were confirmed the apoptosis and autophagy stimulating capacity of the formulated ZnO-Pip-NC in human gastric cancer.

The inflammatory conditions eventually enhance the multiplication and survival of the tumor cells in the early stage. The tumor enhancing cytokines generally accreted by the inflammatory cells and these modulators stimulate transcription factors like STAT-3, NF-ƙB, and activator protein-1 in the vulnerable cells to escalate the expression of survival genes and stimulate the cell multiplication and growth to colonize the tumor cells. The cytokines are playing an imperative function in the cellular and pathological mechanisms. These cytokines can inhibit or enhance tumor development (Heydt et al., 2018). Several inflammatory modulators like IFN-γ and IL-12 exhibited the antitumor capacity; on the other hand, the TNF-α, TGF-β, IL-6, and EGFR ligands were concerned to promote the growth and survival of the tumor cells (Fernandes et al., 2015). The IL-6 and TNF-α are the vital pro-inflammatory modulators that are essential for the cellular signaling and inflammatory mechanisms. Severe inflammatory conditions enhance the initiation and progression of various tumors. The IL-6 and TNF-α are the connective inflammatory modulators that promote multiplication, survival, invasion, metastasis, and tumorigenesis. These cytokines are often accretes the highest levels in the tumor microenvironment in various types of tumors (Ghandadi and Sahebkar, 2016). NF-ƙB is the prime modulator that regulates the critical mechanism between the inflammation and cancer in numerous phases. In cancerous cells along with augmented NF-κB expression, results in the excess accretion of the pro-inflammatory modulators in the tumor tissues eventually develop the pro-tumorigenic microenvironment (Wang et al., 2016). The findings of this current investigation proved that the treatment with the formulated ZnO-Pip-NC to the GC stimulated animals were displayed the noticeable diminution in the pro-inflammatory cytokines i.e. IL-6, TNF-α, and NF-ƙB in the stomach tissues of MNNG-challenged animals.

The influences of excess ROS are well known in numerous fatal ailments, including cancers and it was assuaged by the enzymatic and non-enzymatic antioxidants (Xia et al., 2014). The numerous cellular antioxidants like SOD, CAT, and GSH are playing a critical function in assuaging the excess ROS accretion thereby preventing the ROS induced cellular damages (Marinescu et al., 2014). The GSH is an imperative non-enzymatic antioxidant in most cells. GSH is the most influential antioxidant in the cells, and it is implicated in the detoxification of various electrophilic compounds and

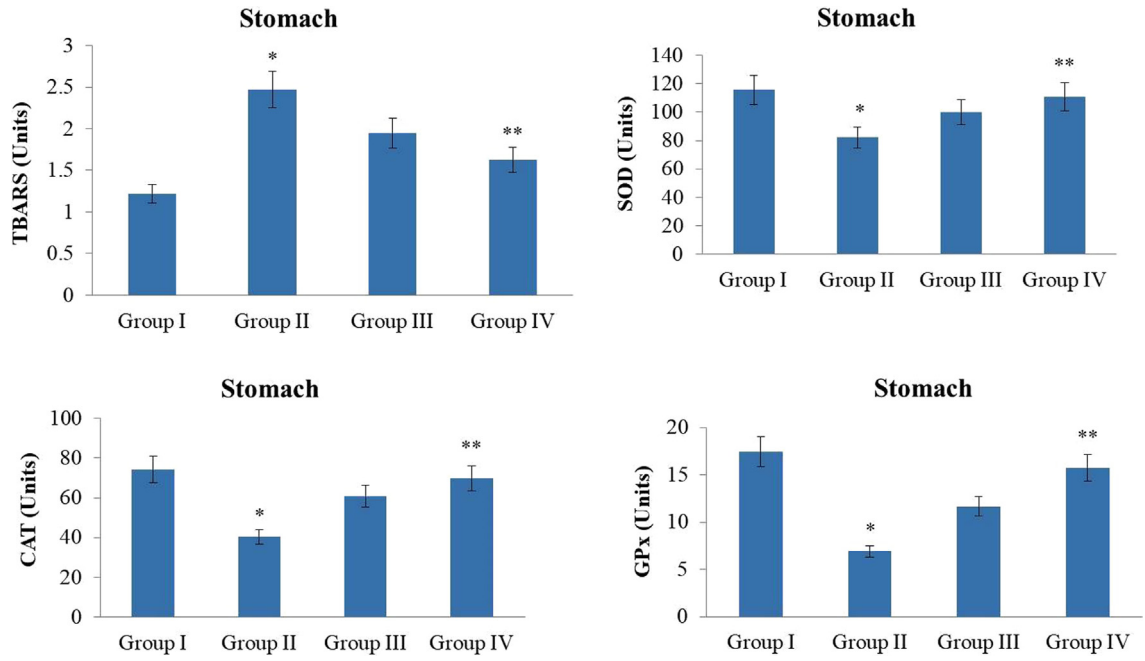

Fig. 11 Effect of synthesized ZnO-Pip-NC on TBARS and antioxidant enzymes level in the experimental animals. The supplementation of10 and 20 mg/kg of ZnO-Pip-NC to the GC induced animals exhibited the noticeable augmentation in the antioxidant enzymes i.e. CAT, SOD, GPx status and diminished the lipid peroxidation level.

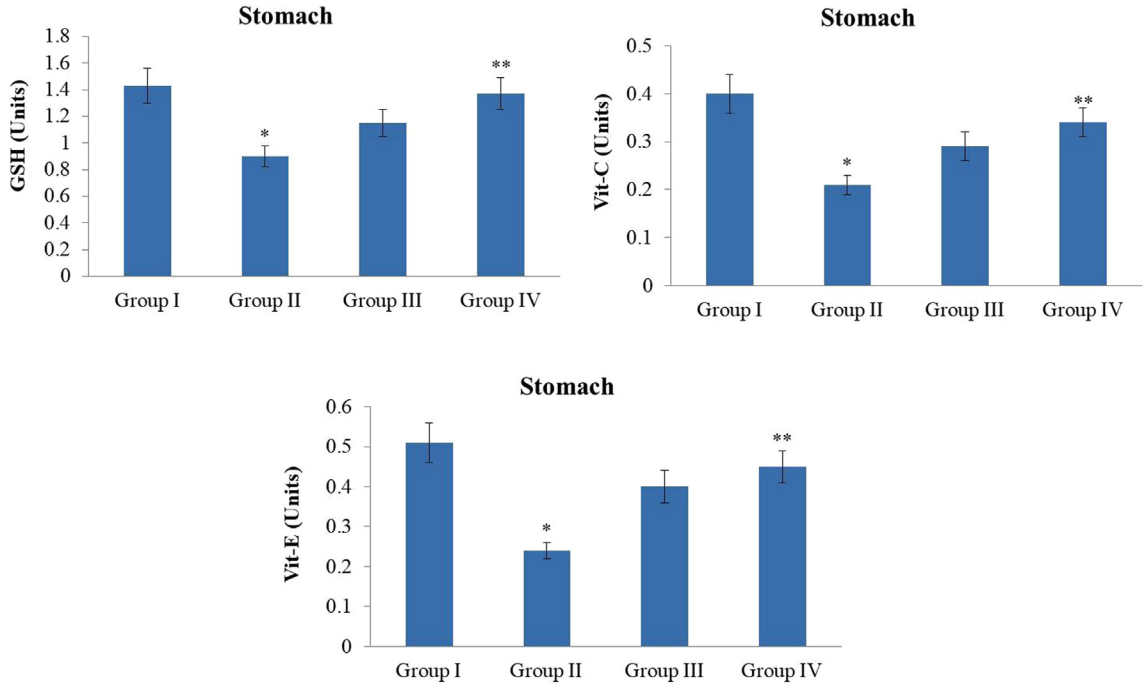

Fig. 12 Effect of synthesized ZnO-Pip-NC on the non-enzymatic antioxidants level in the experimental animals. The treatment with the ZnO-Pip-NC amazingly restored the non-enzymatic antioxidants i.e. vit-E, vit-C, and GSH in the stomach tissues in the GC induced animals.

peroxides under the catalysis of glutathione-s-transferase (GST) and glutathione peroxidase (GPx). The diminution in the enzymatic and non-enzymatic antioxidants can enhance the intracellular ROS status (Oyewole and Birch-Machin, 2015). Furthermore, the non-enzymatic antioxidant like vitamin-C (ascorbic acid) was mentioned to playing the imperative functions in inducing the immune system through alleviating the chronic inflammatory reactions, the diligence of which is concerned in the incidences of the numerous ailments, including cancers (Habermann et al., 2017). In this study, we

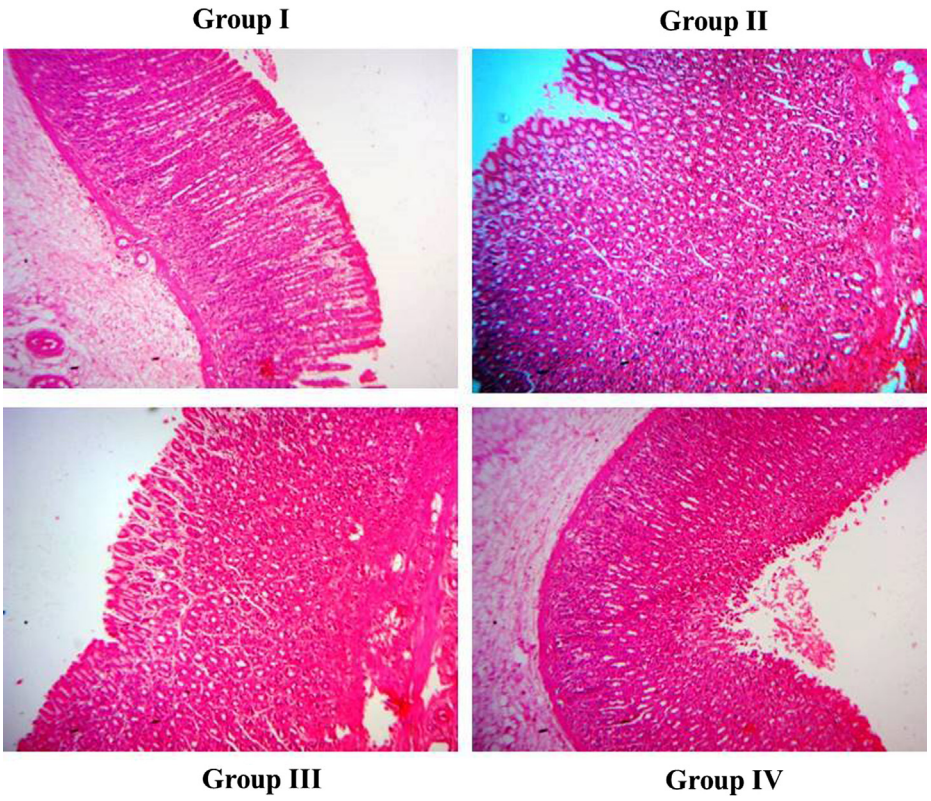

Fig. 13 Effect of ZnO-Pip-NC on histological analysis of gastric mucosa in the experimental animals. Histological investigation proved that the formulated ZnO-Pip-NC treatment to the GC animals has noticeably ameliorated the histological changes and assuaged the tumor burden in the gastric mucosa of experimental animals.

also noted that the MNNG-stimulated GC in animals were exhibited a severe reduction in both enzymatic and non-enzymatic antioxidants in the stomach tissues of GC animals. Interestingly, the fabricated ZnO-Pip-NC supplemented animals were displayed the noticeable regain in the enzymatic (SOD, CAT, and GPx) and non-enzymatic (vit-C, vit-E, and GSH) in the stomach tissues of GC induced animals that proved the potential antioxidant activity of the ZnO-Pip-NC.

The abnormal stimulation of the PI3K-Akt-mTOR signaling pathways was concerned with the numerous carcinomas. The induction of PI3K-Akt-mTOR pathways directs to the escalated cell multiplication, growth, and involvement in angiogenesis, thereby promoting the migration, invasion, and metabolism of the cells (Sorice et al., 2014). The PI3K-Akt-mTOR pathways are the vital cellular signaling cascades that perform a crucial function in the regulation f cell survival, multiplication, metabolism, and apoptosis. It also causes tumorigenesis and enhances cancer metastasis and resistance to chemotherapy drugs (Rosenberg et al., 2018; Wang et al., 2019; Xiong et al., 2017). The enhanced regulation of this signaling cascade is concerned in various malignant tumor tissues, including GC. In GC cells, the induced PI3K leads to the phosphorylation of Akt, thereby enhances the multiplication of GC cells via numerous pathways like mTOR. It also inhibits autophagy and apoptosis in the GC cells and diminishes the sensitivity of GC cells to the chemotherapeutic drugs. The preceding findings were highlighted that the GC patients along with the anomalous stimulation of the PI3K-Akt-mTOR pathways have the reduced prognosis and very minimal survival rate. Consequently, this signaling cascade has turned into the prime target for the exploration of novel therapeutic agents (Lei et al., 2019). The novel findings of this current exploration have confirmed that the fabricated ZnO-Pip-NC treatment to the AGS cells was noticeably inhibited the PI3K/Akt signaling pathway thereby improved the apoptosis and autophagy in the AGS cell line.

5. Conclusion

In conclusion, the novel findings of this current study were proved that the formulated piperine-loaded ZnO nanocomposite (ZnO-Pip-NC) possessed the anticancer activity against GC. The ZnO-Pip-NC treatment appreciably inhibited the AGS cell viability and promoted the apoptosis and autophagy in the AGS cells by inhibiting the apoptotic and PI3K/Akt/mTOR signaling pathway. The *in vivo* studies confirmed the anticancer potential of the formulated ZnO-Pip-NC by its anti-inflammatory and antioxidant abilities. Hence it was clear that the fabricated ZnO-Pip-NC can be utilized to treat the gastric cancer. However, further researches are still needed in the future to elucidate the accurate therapeutic mechanisms of the ZnO-Pip-NC against the GC.

Funding

Provincial Department of Education, Henan, Henan Province Colleges and Universities Key Scientific Research Project Plan (20B320034).

Declaration of Competing Interest

The authors declare that they have no known competing financial interests or personal relationships that could have appeared to influence the work reported in this paper.

References

Abral, H., Ariksa, J., Mahardika, M., Handayani, D., Aminah, I., Sandarwat, N., Pratama, A.B., Fajri, N., Sapuan, S.M., Ilyas, R. A., 2020. Transparent and antimicrobial cellulose film from ginger nanofiber. Food Hydrocolloids 98. 105266.

Aziz, A.U.R., Farid, S., Qin, K., Wang, H., Liu, B., 2018. PIM Kinases and Their Relevance to the PI3K/AKT/mTOR Pathway in the Regulation of Ovarian Cancer. Biomolecules 8.

Bang, J.S., Choi, H.M., Sur, B.J., Lim, S.J., Kim, J.Y., Yang, H.I., Yoo, M.C., Hahm, D.H., Kim, K.S., 2009. Anti-inflammatory and antiarthritic effects of piperine in human interleukin 1β-stimulated fibroblast-like synoviocytes and in rat arthritis models. Arthritis. Res. Ther. 11, R49.

Bray, F., Ferlay, J., Soerjomataram, I., Siegel, R.L., Torre, L.A., Jemal, A., 2018. Global cancer statistics 2018: GLOBOCAN estimates of incidence and mortality worldwide for 36 cancers in 185 countries. CA Cancer J. Clin. 68 (2018), 394–424.

Chen, J.F., Wu, P., Xia, R., Yang, J., Huo, X.Y., Gu, D.Y., Tang, C. J., De, W., Yang, F., 2018. STAT3-induced lncRNA HAGLROS overexpression contributes to the malignant progression of gastric 501 cancer cells via mTOR signal-mediated inhibition of autophagy. Mol. Cancer 17, 6.

Chonpathompikunlert, P., Wattanathorn, J., Muchimapura, S., 2010. Piperine, the main alkaloid of Thai black pepper, protects against neurodegeneration and cognitive impairment in animal model of cognitive deficit like condition of Alzheimer's disease. Food Chem. Toxicol. 48, 798–802.

Clavel, M., Michaeli, S., Genschik, P., 2017. Autophagy: a double-edged sword to fight plant viruses. Trends Plant Sci. 22, 646–648.

Desai, I.D., 1984. Vitamin E analysis methods for animal tissue. Methods Enzymol. 105, 138–142.

Ellman, G.L., 1959. Tissue sulfhydryl groups. Arch. BiochemBiophys. 82, 70–77.

Fernandes, J.V., Cobucci, R.N., Jatoba, C.A., Fernandes, T.A., de Azevedo, J.W., de Araujo, J.M., 2015. The role of the mediators of inflammation in cancer development. Pathol. Oncol. Res. 21, 527–534.

Fu, Z., Cheng, X., Kuang, J., Feng, H., Chen, L., Liang, J., Shen, X., Yuen, S., Peng, C., Shen, B., Jin, Z., Qiu, W., 2018. CQ sensitizes human pancreatic cancer cells to gemcitabine through the lysosomal apoptotic pathway via reactive oxygen species. Mol. Oncol. 12 (4), 529–544.

Galluzzi, L., Pedro, J.M., Demaria, S., Formenti, S.C., Kroemer, G., 2017. Activating autophagy to potentiate immunogenic chemotherapy and radiation therapy. Nat. Rev. ClinOncol. 14 (4), 247–258.

Ghandadi, M., Sahebkar, A., 2016. Interleukin-6: a critical cytokine in cancer multidrug resistance. Curr. Pharm. Des. 22, 518–526.

Greenshields, A.L., Doucette, C.D., Sutton, K.M., Madera, L., Annan, H., Yaffe, P.B., Knickle, A.F., Dong, Z., Hoskin, D.W., 2015. Piperine inhibits the growth and motility of triplenegative breast cancer cells. Cancer Lett. 357, 129–140.

Habermann, K.J., Grünewald, L., Fulda, S., Van, W.S., 2017. Targeting redox homeostasis in rhabdomyosarcoma cells: GSH-depleting agents enhance auranofin-induced cell death. Cell Death Dis. 8 (10). e3067.

Heydt, Q., Larrue, C., Saland, E., Bertoli, S., Sarry, J.E., Besson, A., Manenti, S., Joffre, C., Mansat-De Mas, V., 2018. Oncogenic FLT3-ITD supports autophagy via ATF4 in acute myeloid leukemia. Oncogene 37 (6), 787–797.

Huang, J., Li, G., Zhou, Z., Jiang, Y., Hu, Q., Xue, C., Guo, W., 2018. Efficient photocatalytic hydrogen production over Rh and Nb codoped TiO_2 nanorods. Chem. Eng. J. 337, 82–89.

Huang, L., Liu, M., Huang, H., Wen, Y., Zhang, X., Wei, Y., 2018. Recent advances and progress on melanin-like materials and their biomedical applications. Biomacromolecules 19 (6), 1858–1868.

Huang, H., Liu, M., Jiang, R., Chen, J., Mao, L., Wen, Y., Tian, J., Zhou, N., Zhang, X., Wei, Y., 2018. Facile modification of nanodiamonds with hyperbranched polymers based on supramolecular chemistry and their potential for drug delivery. J. Colloid Inter. Sci. 513, 198–204.

Ilyas, R.A., Sapuan, S.M., Ishak, M.R., Zainudin, E.S., 2018. Development and characterization of sugar palm nanocrystalline cellulose reinforced sugar palm starch bionanocomposites. Carbohydrate Polym. 202, 186–202.

Ilyas, R.A., Sapuan, S.M., Ishak, M.R., 2018. Isolation and characterization of nanocrystalline cellulose from sugar palm fibres (*Arenga pinnata*). Carbohycrate Polym. 181, 1038–1051.

Ilyas, R.A., Sapuan, S.M., Ishak, M.R., Zainudin, E.S., 2019. Sugar palm nanofibrillated cellulose (*Arenga pinnata (Wurmb.)Merr*): Effect of cycles on their yield, physic-chemical, morphological and thermal behaviour. Int. J. Biol. Macromolecule 123, 379–388.

Ilyas, R.A., Sapuan, S.M., Ibrahim, R., Abral, H., Ishak, M.R., Zainudin, E.S., Asrofi, M., Atikash, M.S.N., Huzaifah, M.R.M., Radzi, A.M., Azammi, A.M.N., Shaharuzaman, M.A., Nurazzi, N. M., Syafri, E., Sari, N.H., Norrrahim, M.N.F., Jumaidin, R., 2019. Sugar palm (*Arenga pinnata (Wurmb.)Merr*) cellulosic fibre hierarchy: a comprehensive approach from macro to nano scale. J. Mater. Res. Tech. 8 (3), 2753–2766.

Jeong, D.Y., Kim, Kang, S.H., Yun, H.K., Kim, J.L., Kim, B.R., Park, S.H., Na, Y.J., Jo, M.J., Jeong, Y.A., Kim, B.G., Lee, D.H., Oh, S.C., 2019. Docosahexaenoic acid enhances oxaliplatin-induced autophagic cell death via the ER Stress/Sesn2 pathway in colorectal cancer. Cancers (Basel) 11.

Kakkar, P., Das, B., Viswanathan, P.N., 1984. A modified spectroscopic assay of superoxide dismustase. Indian J. Biochem. Biophys. 21, 130–132.

Katai, H., Ishikawa, T., Akazawa, K., Isobe, Y., Miyashiro, I., Oda, I., Tsujitani, S., Ono, H., Tanabe, S., Fukagawa, T., Nunobe, S., Kakeji, Y., Nashimoto Registration Committee of the Japanese Gastric Cancer, A, A., 2018. Five-year survival analysis of surgically resected gastric cancer cases in Japan: a retrospective analysis of more than 100,000 patients from the nationwide registry of the Japanese Gastric Cancer Association. Gastric Cancer 21 (2001–2007), 144–154.

Kim, K.Y., Park, K., Kim, S.H., Yu, S.N., Park, S.G., Kim, Y.W., Seo, Y.K., Ma, J.Y., Ahn, S.C., 2017. Inhibition of autophagy promotes salinomycin-induced apoptosis via reactive oxygen species-mediated PI3K/AKT/mTOR and ERK/p38 MAPK-Dependent signaling in human prostate Cancer cells. Int. J. Mol. Sci. 18, 1088.

King, D., Yeomanson, D., Bryant, H.E., 2015. PI3King the lock: targeting the PI3K/Akt/mTOR pathway as a novel therapeutic strategy in neuroblastoma. J. PediatrHematolOncol. 37, 245–251.

Kinsey, C.G., Camolotto, S.A., Boespflug, A.M., Guillen, K.P., Foth, M., Truong, A., Schuman, S.S., Shea, J.E., Seipp, M.T., Yap, J.T., Burrell, L.D., Lum, D.H., Whisenant, J.R., Gilcrease, G.W., Cavalieri, C.C., Rehbein, K.M., Cutler, S.L., Affolter, K.E., Welm, A.L., Welm, B.E., Scaife, C.L., Snyder, E.L., McMahon, M., 2019. Publisher Correction: protective autophagy elicited by RAF–>MEK–>ERK inhibition suggests a treatment strategy for RAS-driven cancers. Nat. Med. 25, 861.

Lam, K., Law, B., Chan, W., Wong, Y., Chiu, K., So, T., Chan, S., Lee, V., Chu, K., Kwong, D., Law, S., 2018. Feasibility study of intraperitonealdocetaxel combined with intravenous cisplatin and oral S-1 for gastric cancer patients with peritoneal carcinomatosis. Ann. Oncol. 29.

Lei, B., Sun, S., Zhang, X., Feng, C., Xu, J., Wen, Y., Huang, Y., Wu, M., Yu, Y., 2019. Bisphenol AF exerts estrogenic activity in MCF-7 cells through activation of Erk and PI3K/Akt signals via GPER signaling pathway. Chemosphere 220, 362–370.

Liu, M., Ji, J., Zhang, X., Zhang, X., Yang, B., Deng, F., Li, Z., Wang, K., Yang, Y., Wei, Y., 2015. Self-polymerization of dopamine and polyethyleneimine: novel fluorescent organic nanoprobes for biological imaging applications. J. Mater. Chem. B. 3 (17), 3476–3482.

Liu, J., Lam, J.W.Y., Tang, B.Z., 2009. Acetylenic polymers: syntheses, structures, and functions. Chem. Rev. 109 (11), 5799–5867.

Liu, M., Zeng, G., Wang, K., Wan, Q., Tao, L., Zhang, X., Wei, Z., 2016. Recent developments in polydopamine: an emerging soft matter for surface modification and biomedical applications. Nanoscale 8 (38), 16819–16840.

Mao, Q.Q., Huang, Z., Zhong, X.M., Xian, Y.F., Ip, S.P., 2014. Brain-derived neurotrophic factor signalling mediates the antidepressant-like effect of piperine in chronically stressed mice. Behav. Brain Res. 261, 140–145.

Marinescu, S., Anghel, R., Gruia, M.I., Beuran, M., 2014. Involvement of reactive oxygen species in the mechanisms associated with cervical cancer specific treatment. Chirurgia (Bucur) 109, 806–811.

Mishra, P.K., Mishra, H., Ekielski, A., Talegaonkar, S., Vaidya, B., 2017. Zinc oxide nanoparticles: a promising nanomaterial for biomedical applications. Drug Discovery Today. 22 (12), 1825–1834.

Niehius, W.G., Samuelson, B., 1968. Formation of malondialdehyde from phospholipid arachidonate during microsomal lipid peroxidation. Eur. J. Biochem. 6, 126–130.

Nienhuser, H., Schmidt, T., 2018. 9 weeks that matter for patients with gastric cancer. Lancet Oncol. 19 (11), 1418–1419.

Omaye, S.T., Turnbull, J.D., Sauberlich, H.E., 1979. Selected methods for the determination of ascorbic acid in animal cells, tissues and fluids. Methods Enzymol. 62, 3–11.

Ouyang, D.Y., Zeng, L.H., Pan, H., Xu, L.H., Wang, Y., Liu, K.P., He, X.H., 2013. Piperine inhibits the proliferation of human prostate cancer cells via induction of cell cycle arrest and autophagy. Food Chem. Toxicol. 60, 424–430.

Oyewole, A.O., Birch-Machin, M.A., 2015. Mitochondria-targeted antioxidants. FASEB J. 29, 4766–4771.

Ramirez, R.E.H., Lijanova, I.V., Likhanova, N.V., Xometl, O.O., Herrera, A.H., Alcala, J.F.C., Chavero, O.T., 2020. Synthesis of PAMAM dendrimers with porphyrin core and functioned periphery as templates of metal composite materials and their toxicity evaluation. Arab. J. Chem. 13 (1), 27–36.

Reda, S.M., Khairy, M., Mousa, M.A., 2020. Photocatalytic activity of nitrogen and copper doped TiO_2 nanoparticles prepared by microwave-assisted sol-gel process. Arab. J. Chem. 13 (1), 86–95.

Ren, T., Wang, Q., Li, C., Yang, M., Zuo, Z., 2018. Efficient brain uptake of piperine and its pharmacokinetics characterization after oral administration. Xenobiotica 48, 1249–1257.

Rosenberg, L., Yoon, C.H., Sharma, G., Bertagnolli, M.M., Cho, N. L., 2018. Sorafenib inhibits proliferation and invasion in desmoid-derived cells by targeting Ras/MEK/ERK and PI3K/Akt/mTOR pathways. Carcinogenesis 39, 681–688.

Rotruck, J.T., Pope, A.L., Ganther, H.E., 1973. Selenium: biochemical role as a component of glutathione peroxidase purification assay. Sci. 179, 588–590.

Ruszkiewicz, J.A., Pinkas, A., Ferrer, B., Peres, T.V., Tsatsakis, A., Aschner, M., 2017. Neurotoxic effect of active ingredients in sunscreen products, contemporary review. Toxicol Rep. 4, 245–259.

Shi, Y., Liu, M., Deng, F., Zeng, G., Wan, Q., Zhang, X., Wei, Y., 2017. Recent progress and development on polymeric nanomaterials for photothermal therapy: a brief overview. J. Mater. Chem. B 5 (2), 194–206.

Shi, Y., Jiang, R., Liu, M., Fu, L., Zeng, G., Wan, Q., Mao, L., Deng, F., Zhang, X., Wei, Y., 2017. Facile synthesis of polymeric fluorescent organic nanoparticles based on the self-polymerization of dopamine for biological imaging. Mater. Sci. Eng.: C 77 (1), 972–977.

Siegel, R.L., Liang, T., Shi, M., 2016. Cancer statistics, 2016. CA Cancer J Clin. 66 (1), 7–30.

Sinha, A.K., 1972. Colorimetric assay of catalase. Anal. Biochem. 47, 389–394.

Song, P., Jiang, B., Liu, Z., Ding, J., Liu, S., Guan, W., 2017. A three-lncRNA expression signature associated with the prognosis of gastric cancer patients. Cancer Med. 6, 1154–1164.

Sorice, A., Guerriero, E., Capone, F., Colona, G., Castello, G., Costantini, S., 2014. Ascorbic acid: its role in immune system and chronic inflammation diseases. Mini Rev. Med. Chem. 14, 444–452.

Syafri, E., Sudirman, Mashadi, Yulianti, E., Deswita, Asrofi, M., Abral, H., Sapuan, S.M., Ilyan, R.A., Fudholi, A., 2019. Effect of sonication time on the thermal stability, moisture absorption, and biodegradation of water hyacinth (*Eichhornia crassipes*) nanocellulose-filled bengkuang (*Pachyrhizus erosus*) starch biocomposites. J. Mater. Res. Tech. 8 (6), 6223–6231.

Torre, A., Bray, F., Siegel, R.L., Ferlay, J., Lortet-Tieulent, J., Jemal, A., 2015. GLobal cancer statistics, 2012. CA: a Cancer J. Clin. 65 (2), 87–108.

Wan, Q., Huang, Q., Liu, M., Xu, D., Huang, H., Zhang, X., Wei, Y., 2017. Aggregation-induced emission active luminescent polymeric nanoparticles: Non-covalent fabrication methodologies and biomedical applications. Appl. Mater. Today 9, 145–160.

Wang, K., Chu, D., Wu, J., Zhao, M., Zhang, M., Li, B., Du, W., Du, J., Guo, R., 2019. Cinobufagin induced cell apoptosis and protective autophagy through the ROS/ MAPK signaling pathway. Life Sci. 116642.

Wang, X., Pan, J., Liu, D., Zhang, M., Li, X., Tian, J., Liu, M., Jin, T., An, F., 2019. Nicorandil alleviates apoptosis in diabetic cardiomyopathy through PI3K/Akt pathway. J. Cell Mol. Med. 23, 5349–5359.

Wang, C.X., Williams, G.M., 1987. Comparison of stomach cancer induced in rats by N-methyl-N;-nitro-N-nitrosoguanidine of N-propyl-N'-nitro-N-nitrosoguanidine. Cancer Lett. 34(2), 173–185.

Wang, Y., Yi, J., Chen, X., Zhang, Y., Xu, M., Yang, Z., 2016. The regulation of cancer cell migration by lungcancer cell-derived exosomes through TGF-beta and IL-10. Oncol. Lett. 11. 1527e1530.

Xia, Y., Shen, S., Verma, I.M., 2014. NF-kB, an active player in human cancers. Cancer Immunol. Res. 2 (9), 823–830.

Xiong, J., Wang, D., Wei, A., Lu, H., Tan, C., Li, A., Tang, J., Wang, Y., He, S., Liu, X., Hu, W., 2017. Deregulated expression of miR-107 inhibits metastasis of PDAC through inhibition PI3K/Akt signaling via caveolin-1 and PTEN. Exp. Cell Res. 361, 316–323.

Yaffe, P.B., Power Coombs, M.R., Doucette, C.D., Walsh, M.M., Hoskin, D.W., 2015. Piperine, an alkaloid from black pepper, inhibits growth of human colon cancer cells via G1 arrest and apoptosis triggered by endoplasmic reticulum stress. Mol. Carcinog. 54, 1070–1085.

Yao, Y., Lu, Q., Hu, Z., Yu, Y., Chen, Q., Wang, Q.K., 2017. A non-canonical pathway regulates ER stress signaling and blocks ER stress-induced apoptosis and heart failure. Nat. Commun. 8 (1), 133.

Yu, Y., Wu, X., Pu, J., Luo, P., Ma, W., Wang, J., Wei, J., Wang, Y., Fei, Z., 2018. *Lyciumbarbarum* polysaccharide protects against oxygen glucose deprivation/reoxygenationinduced apoptosis and autophagic cell death via the PI3K/Akt/mTOR signaling pathway in primary cultured hippocampal neurons. Biochem. Biophys. Res. Commun. 495, 1187–1194.

Zhang, X., Zhang, X., Yang, B., Liu, M., Liu, W., Chen, Y., Wei, Y., 2014. Fabrication of aggregation induced emission dye-based fluorescent organic nanoparticles via emulsion polymerization and their cell imaging applications. Polym. Chem. 5 (2), 399–404.

Zhang, X., Zhang, X., Yang, B., Liu, M., Liu, W., Chen, Y., Wei, Y., 2014. Polymerizable aggregation-induced emission dye-based fluo-

rescent nanoparticles for cell imaging applications. Polym. Chem. 5 (2), 356–360.

Zhang, X., Wang, K., Liu, M., Zhang, X., Tao, L., Chen, Y., Wei, Y., 2015. Polymeric AIE-based nanoprobes for biomedical applications: recent advances and perspectives. Nanoscale 7 (27), 11486–11508.

Zheng, T., Yang, X., Wu, D., Xing, S., Bian, F., Li, W., Chi, J., Bai, X., Wu, G., Chen, X., Zhang, Y., Jin, S., 2015. Salidroside ameliorates insulin resistance through activation of a mitochondria-associated AMPK/PI3K/Akt/GSK3beta pathway. Br. J. Pharmacol. 172 (13), 3284–3301.